PAPER

Adsorbate enhancement of electron emission during the quenching of metastable CO at metal surfaces

Daniel P. Engelhart,[ab] Roman J. V. Wagner,[ab] Peter C. Johnsen,[c] Alec M. Wodtke[ab] and Tim Schäfer*[ab]

When electronically excited CO($a^3\Pi$) collides with a Au(111) surface, electron emission can be observed with a quantum efficiency of 0.13. We have studied the influence of Ar, Kr and Xe adsorption on the electron emission efficiency resulting from CO($a^3\Pi$) quenching. Surprisingly, a single monolayer (ML) of rare gas dramatically enhances electron emission. For Ar and Kr bilayers, emission efficiency is further enhanced and approaches unity. The quenching mechanism involves electron transfer from the metal to the CO($a^3\Pi$) molecule followed by electron emission from the molecule. The enhanced emission efficiency is due to the long range nature of the initial electron transfer process and the rare gas adlayer's ability to reflect the electron emitted by the transient CO anion. This work shows that CO($a^3\Pi$) quenching is a useful model system for investigating the fate of electronically excited molecules at surfaces.

Introduction

When electronically excited molecules collide with metal surfaces, electron transfer (ET) between surface and molecule often occurs, which can be accompanied by electron emission into vacuum.[1–5] We studied the interaction of electronically excited CO molecules in the $a^3\Pi$ state – hereafter referred to as CO* – with a Au(111) surface using molecular beam surface scattering experiments.[3,4] CO* molecules exhibit an internal electronic excitation energy of 6.0 eV, and electron emission is observed when CO* collides with a Au(111) surface with a work function $\Phi_{Au} = 5.3$ eV.[3]

We found that the quenching mechanism of CO* at Au(111) is mediated by the formation of a transient anionic shape resonance.[3,4] The key step in the process is the ET from the surface to the incident molecule, which is dependent on the overlap of the molecule's free orbitals with the conduction band wave functions of the metal. In contrast to an Auger mediated mechanism, which is a simultaneous two-electron transition, the de-excitation *via* a short-lived shape resonance and subsequent electron auto-detachment consists of two, sequential one-electron steps. Fig. 1 schematically displays the underlying mechanism. Naturally, the measured electron
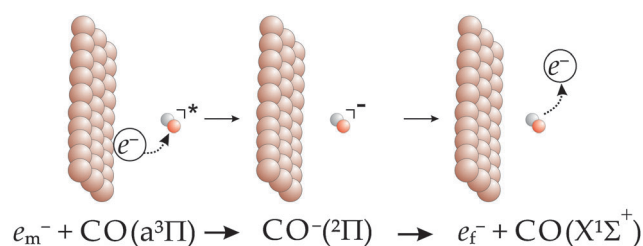

$$e_m^- + CO(a^3\Pi) \longrightarrow CO^-(^2\Pi) \longrightarrow e_f^- + CO(X^1\Sigma^+)$$

Fig. 1 De-excitation of metastable CO*($a^3\Pi$) *via* an anion mediated mechanism. In the first step an electron is transferred resonantly from the surface to the molecule. The anion subsequently decays to the electronic ground state by an auto-detachment mechanism on a fs timescale.

yield depends on the efficiency of both steps: the electron transfer efficiency from the surface to the metastable and the subsequent electron emission efficiency.

The electron transfer efficiency from the metal to the molecule and the lifetime of the resulting anion depend strongly on the distance between surface and molecule. A means to probe these surface distance effects is the introduction of rare gas layers between metal surface and gas phase molecules, as has been successfully employed in two photon photoemission (2PPE) studies by Hotzel *et al.*[6] However, the introduction of a "spacer layer" not only influences the interaction distance, it can also lead to a significant change of the surface work function.[7] Furthermore, there has been little work describing the influence of the spacer layer on electron emission efficiency.

In this paper, we systematically probe the influence of surface adsorbate coverage on the de-excitation process for the CO*–Au(111)

[a] *Institut für Physikalische Chemie, Georg-August University of Göttingen, Tammannstraße 6, 37077 Göttingen, Germany. E-mail: tschaef4@gwdg.de*

[b] *Department of Dynamics at Surfaces, Max Planck Institut für biophysikalische Chemie, am Faßberg 11, 37077 Göttingen, Germany*

[c] *Department of Physics, Princeton University, Princeton, New Jersey, USA*

11540 | *Phys. Chem. Chem. Phys.*, 2015, **17**, 11540–11545

This journal is © the Owner Societies 2015

system by controlled adsorption of Ar, Kr, and Xe. The non-reactive adsorbates serve as a spacer between the metal surface and colliding molecule. Thus, the range of interaction distances between the metal surface and the impinging molecule can be controlled directly. One might expect the electron emission yield to decrease with increasing spacer layer thickness as electron transfer efficiency can be reduced due to decreasing overlap between electron wave functions of surface and molecule at increased surface distance. However, this is only observed for very thick over-layers. Surprisingly, the electron emission yield increases markedly when adsorbing rare gas monolayers on the surface. By carefully adjusting coverage, the emission probability can be enhanced to near unity for Ar and Kr adsorbates. We explain this remarkable behavior by an enhanced electron reflection probability at the surface induced by rare gas adsorption.

Experimental

Quenching of metastable CO* molecules on a Au(111) surface has been performed in an ultra-high vacuum (UHV) surface science chamber combined with a differentially pumped molecular beam setup. A detailed description of the machine can be found in ref. 10. We briefly describe the experiment here. A molecular beam of metastable CO* molecules is created by expanding 20% CO in xenon in a pulsed valve (General Valve series 99) cooled to 260 K and subsequently collimated with a skimmer (Beam Dynamics Model 2, Ni). Directly after the skimmer, electronic ground state CO molecules are excited to the $a^3\Pi$ state by means of a home-built narrow bandwidth pulsed injection seeded optical parametric oscillator laser system.[8] The laser system provides 2 mJ of 206 nm light with a bandwidth of 300 MHz, enough to transfer sufficient molecules to the metastable state via the $a^3\Pi_1$ ($v = 0, J = 1$) ← $X^1\Sigma^+$ ($v = 0, J = 1$) transition.

Metastable CO* molecules exhibit a lifetime of 2.6 ms and a dipole moment of 1.37 Debye.[9] They are separated from the carrier gas by deflection in an electrostatic hexapole filter, which is tilted by 3.5° with respect to the expansion axis of the pulsed valve. Subsequently, the pulse of CO* molecules is guided at 360 m s^{-1} through a 131 stage Stark decelerator before it enters the UHV chamber via a 2 mm diameter aperture. Here, the metastable CO* molecules are scattered from the Au(111) surface and electrons emitted at the surface are detected on a dual microchannel plate detector (MCP, tectra Physikalische Instrumente, GmbH, MCP 050, 40 mm, chevron configuration).

The UHV chamber is maintained at a base pressure of 10^{-10} mbar, and is equipped with a Ne-ion gun and an Auger spectrometer. The surface is prepared with standard sputter–anneal cycles with 19 μA surface ion current and 900 K anneal temperature. Surface purity is confirmed with Auger electron spectroscopy. The gold crystal is mounted at the end of an oxygen free high-conductivity (OFHC) copper cold finger and can be temperature controlled between 19 K and 1360 K by means of a closed cycle helium cryostat (Advanced Research Systems, Inc. CS204B) and resistive heating. The temperature is monitored with a chromel/constantan (type E, Omega) thermocouple mounted directly in

the gold crystal. Translation and rotation of the crystal in the UHV chamber are accomplished by means of dual rotary feedthroughs (VG Scienta ZRP100H, DN 100CF, Thermionics RNN-1000/MS 13.25''CF) and a 3-axis manipulator (VG Scienta Omniax MXZ800 and MT211B6S).

Controlled coverage of the surface by rare gas adsorbates is achieved employing a leak valve (MDC Precision Leak, DN40CF/DN16CF) to produce defined surface exposures at 19 K surface temperature. Temperature programmed desorption (TPD) measurements have been performed using a quadrupole mass spectrometer (QMS, RGA 200, Stanford Research Systems) mounted in a copper cap with a 1 mm orifice. The front surface of the crystal was moved to within 1.5 mm of the orifice to suppress contributions to the QMS signal from the sample holder, heating wires, crystal rim, etc. during heating. Computer controlled resistive heating allows heating rates between 5 and 90 K min^{-1} using a high current power supply (TDK-Lambda Genesys 8-180) controlled with a proportional feedback system programmed using LABView.

The UHV chamber is constructed in a two level structure. The upper level contains Ne-ion gun, Auger spectrometer, Kelvin probe, leak valve manifold and TPD mass spectrometer. In the upper level, the surface is prepared with well-defined adsorbate coverages. The lower level is used for molecular beam scattering and charged particle detection.

We systematically prepare well-defined layers of rare gas adsorbed on a Au(111) surface by controlled dosing at 19 K and subsequent temperature programmed desorption. Surface adsorbate coverage is determined by integrating the TPD spectra and normalizing to the monolayer peak integral. Low Energy Electron Diffraction (LEED) experiments show that xenon binds at low-coordination sites.[11] See Fig. 2. For argon and krypton no explicit study of the Au(111) surface has been performed; for Ar and Kr on Au(111), we assume structures similar to those that have been experimentally investigated, like Ar and Kr on Ag(111) and Ru(0001).[11]

By adsorption of further rare gas layers on top of the monolayer, we increase the distance of closest possible approach between the metal surface and the incoming molecule. Since rare gases crystallize in a close-packed structure,[12,13] the surface distance induced by the rare gas spacers can be calculated using van der Waals radii. See Table 1.

This precise information about the coverage of the surface is subsequently employed to interpret electron emission measurements resulting from scattering metastable CO* from prepared surfaces.

Results

The influence of rare gas adsorption on the CO* quenching-induced electron emission yield is shown in Fig. 3. Here, we have first dosed the Au(111) surface at 19 K with a well-defined exposure of rare gas to produce >5 ML coverage. The temperature of the gold crystal is then raised at a constant rate while the electron emission resulting from a constant flux of CO* is detected by an MCP. See panels b, d and f. In a separate series
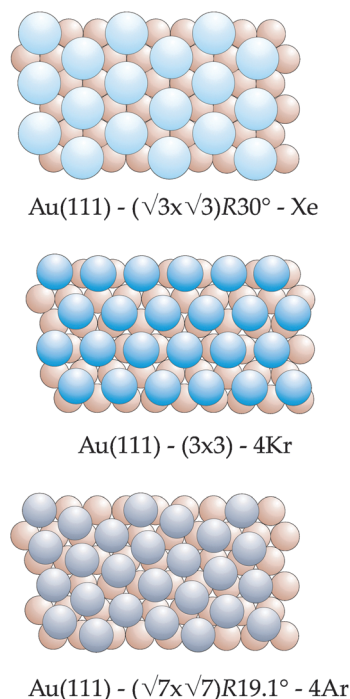
This journal is © the Owner Societies 2015

Phys. Chem. Chem. Phys., 2015, **17**, 11540–11545 | **11541**

Fig. 2 Adsorption geometry for xenon, krypton and argon on a Au(111) surface. Due to the lack of experimental data we assume the argon and krypton adsorption geometry on Au(111) to be similar to the adsorption geometry on similar close-packed transition metal surfaces.

Table 1 Increased distance between metal surface and impinging molecule induced by adsorption of layers of rare gas spacers. The distances have been calculated using van der Waals radii between the atoms' center of mass and assuming close-packing of the rare gases

Argon	
1st layer	3.76 Å
2nd layer	6.54 Å
3rd layer	9.32 Å
Krypton	
1st layer	4.04 Å
2nd layer	7.03 Å
3rd layer	10.01 Å
Xenon	
1st layer	4.32 Å
2nd layer	7.52 Å
3rd layer	10.71 Å

Fig. 3 TPDs (a, c, e) and electron emission curves (b, d, f) for Ar, Kr and Xe adsorbed on a Au(111) surface. During all scans the heating rate was 10 K min^{-1} and the initial coverages >5 ML for Ar/Au(111), Kr/Au(111) and Xe/Au(111), respectively. For all TPDs, α indicates the overlayer peak, β the bilayer peak and γ the monolayer peak. The initial coverage of the electron emission curves was >5 ML in each case. The change in the electron emission curve can be directly correlated to desorption of adsorbate layers at the surface.

of experiments, conventional TPD is performed for comparison – panels a, c, and e.

We note two obvious features. First, all measurements show the same electron yield at the highest surface temperatures, *i.e.* once the rare gas has been removed from the surface, all experiments show the electron emission from a clean gold surface, the absolute yield of which (0.13 ± 0.04) has been previously reported[3] and is used to set the *y*-axis scale in Fig. 3 panels b, d and f. The second obvious feature is that no electron emission is seen at the lowest surface temperatures indicating that rare gas multilayers – when thick enough – completely suppress electron emission.
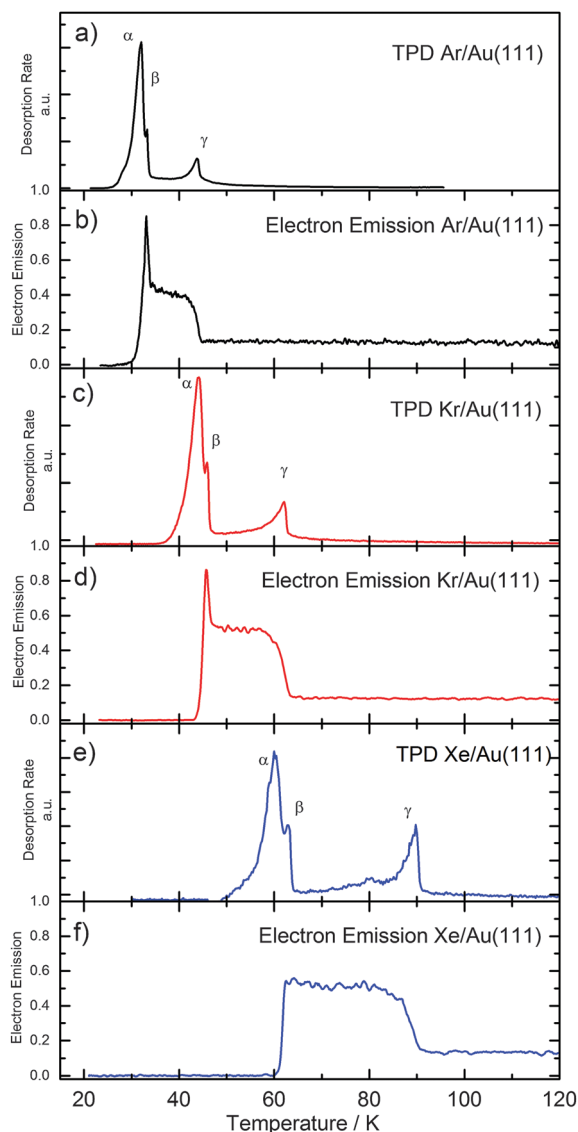
By comparing the temperature dependence of electron emission to controlled TPD spectra, we gain a clear picture of the influence of rare gas adsorption on electron emission probability. In describing rare gas adsorbate layers we refer to: (1) the 1st layer, which is bound directly to the metal, (2) the 2nd layer, which bound to the 1st layer and (3) the outer layers, which are the rest of the adsorbed rare gas. The TPD spectra of all three rare gas adsorbate samples exhibit three clear features, labeled α, β, γ. The peak labeled α occurs at lowest surface temperature and reflects desorption of the most weakly bound outer adsorbate layers. The β feature represents desorption of the more strongly bound 2nd layer and the γ feature reflects
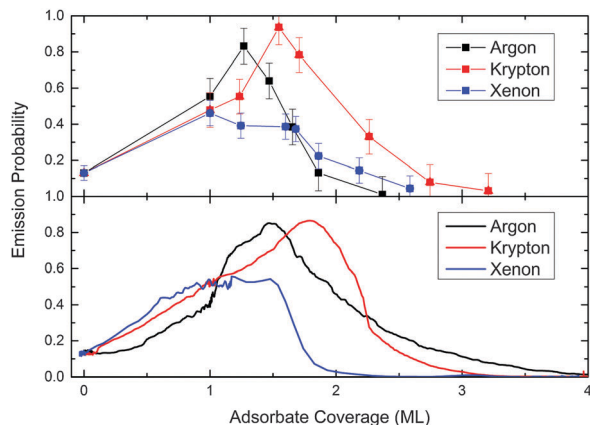
Fig. 4 The upper panel shows the electron emission probability *versus* adsorbate coverage for argon, krypton, and xenon. Lines are added to guide the eye. Error bars are applied reflecting the uncertainty associated with multiple measurements of monolayer enhancement as presented in Table 2. The lower panel shows the electron emission probability *versus* coverage calculated by correlating a TPD spectrum with a temperature programmed electron emission scan for each adsorbate species. See text for more details.

desorption of the 1st layer. For all three rare gases, electron emission appears only as the 2nd layer begins to be exposed, that is, upon outer layer desorption ($T > \alpha$). For Ar and Kr we also see an abrupt decrease in electron emission yield as the 2nd layer sublimates, exposing the 1st layer. This shows how sensitive the electron emission yield is to the atomic structure of the interface.

In order to derive quantitative information about the coverage dependence of electron emission probability, we determined instantaneous coverage at a given temperature by integrating under a TPD scan and normalizing to the integral under a monolayer. By correlating the instantaneous coverage with the electron emission value for the corresponding temperature the electron emission probability is determined as a function of coverage. Results of this analysis are shown in the lower panel of Fig. 4.

To experimentally confirm the validity of this analysis, we measured electron emission from several surfaces prepared with different well-defined adsorbate coverages of argon, krypton and xenon. As surface coverage is determined with TPD, each of these experiments determines the electron emission probability at only a single coverage. See upper panel of Fig. 4.

Both panels of Fig. 4 reveal similar results, lending credence to our analysis. The absolute electron yields are remarkably high in all cases. For argon and krypton covered surfaces, emission probability approaches unity between one and two monolayer coverage. Xenon does not exhibit further enhancement beyond one monolayer. Table 2 summarizes the monolayer emission probability.

Table 2 Absolute electron emission probability for CO* quenching on monolayer covered RG/Au(111) with RG = Ar, Kr, Xe

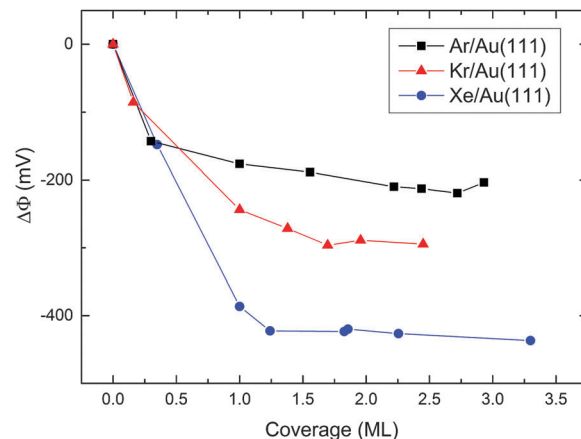| Adsorbate	Emission probability
Ar	0.56 ± 0.10
Kr	0.48 ± 0.10
Xe	0.46 ± 0.07

Fig. 5 Work function change of the Au(111) surface due to the adsorption of rare gas. The work function drops strongly with the adsorption of one monolayer. The effect of any further adsorbed gas is minor. Lines are added to guide the eye.

Adsorption of rare gas layers induces a decrease in the surface work function.[7] Since the anion mediated de-excitation mechanism of CO* at a Au(111) surface depends on the potential energy of involved orbitals, a careful consideration of the influence of changing work function is necessary. The effect of rare gas coverage on the work function is shown in Fig. 5.

The measured work function change is in good agreement with previous measurements.[7] The work function shift induced by a monolayer of Ar, Kr and Xe is 180, 250, and 380 mV, respectively. Due to the increasing polarizability of the noble gases going down the periodic table, Xe atoms induce a larger surface dipole moment than Kr and Ar atoms, leading directly to a larger work function change.

Discussion

We discuss the influence of rare gas adsorption on the electron emission signal based on the electron transfer mediated auto-detachment mechanism described in detail in a previous paper.[4] In this mechanism, electron emission proceeds in two steps. First, an electron is transferred to the CO* molecule when its bond is extended from the equilibrium internuclear distance (CO$^-$ shape resonance). The electron is subsequently emitted from the CO molecule after the bond recompresses leaving the CO molecule in its ground electronic state and the excess electronic excitation with the emitted electron. Two main points must be considered for a complete discussion, namely the influence of the work function change on the mechanism's first step (ET) and the effect of the surface morphology on the mechanism's second step (auto-detachment). We exclude Penning ionization from rare gas adsorbates due to the high ionization energy of rare gases.

Since the de-excitation mechanism of electronically excited molecules depends on the work function of the substrate, any work function change might also affect the de-excitation probability.[5,14] In particular, lowering the surface work function

directly influences the first step of the anion mediated de-excitation mechanism, *i.e.* the ET from the surface to the metastable molecule. Due to the decreased energy barrier between Fermi level electrons and the molecular orbitals, tunneling to the incident molecule becomes more likely for low work function surfaces.[5] Yet, we do not observe this expected behavior in the experimental results. The work function change scales with the polarizability of the rare gas: Xe > Kr > Ar. See Fig. 5. However, the measured monolayer electron emission yield relative to the clean surface exhibits the opposite trend: Ar > Kr > Xe. See Table 2.

It is also important to notice (Fig. 5) that the adsorption of a second atomic layer decreases the work function only slightly compared to the monolayer induced shift for Ar, Kr and Xe. In contrast, the electron emission signal for Ar and Kr covered Au(111) increases by a factor of 1.8 beyond the monolayer signal as the coverage increases beyond one monolayer (Fig. 4). We therefore conclude that the adsorbate induced change of the work function cannot explain the observed electron emission yield enhancement when scattering CO* from adsorbate covered Au(111) surfaces.

It appears more likely that adsorbate enhancement results from an increased efficiency of electron emission from the anion to vacuum. After ET from the surface to the molecule has occurred, the very short lived shape resonance ($\tau \sim 10$ fs) decays to the CO ground electronic state and emits the electron. This occurs when the molecule is still at distances larger than ~ 5 Å.[4] Simple statistical considerations based on the planar symmetry of the system suggest that half of the emitted electrons will be emitted from the anion toward vacuum, and half toward the surface. Please note that this simple picture ignores possible image charge effects on the free electron. Electrons ejected in the direction of the surface can either be absorbed (going undetected) or reflected (to vacuum where they can be observed in this experiment). Hence, the observations of this work support the idea that rare gas adsorption increases the electron reflection probability. The fact that electron emission is completely quenched upon adsorption of a third atomic layer can be explained by considering the closest packed structure of the adsorbate atoms. Two layers of rare gas spacer still leave small holes through the adsorbate layer through which efficient electron transfer can be expected. A third adsorbate layer plugs these holes.

It is known from LEED studies on hydrogen covered tungsten surfaces that elastic backscattering of electrons with low kinetic energies depends strongly on the surface coverage.[15] In particular at electron kinetic energies below 3 eV, the electron reflection probability is drastically enhanced for the adsorbate covered surface compared to the clean surface. See Fig. 2 of ref. 15. The auto-detached electrons from CO^- have kinetic energies in the range of ~ 1 eV.

The rare gas trends seen in this work can also be explained by this hypothesis. Argon, krypton and xenon show different 2D adsorption geometries resulting from the large differences in their van der Waals radii. See Fig. 2. Argon adsorbs more densely $((\sqrt{7} \times \sqrt{7})R19.1° - 4Ar)$ than krypton $((3 \times 3) - 4Kr)$ and xenon $((\sqrt{3} \times \sqrt{3})R30° - Xe)$.[11] The monolayer adsorption structures lead to a trend in how the rare gases obscure the gold surface – argon (most), krypton (less) and xenon (least). This can be seen quantitatively by considering the fraction of substrate metal surface obscured by spheres with radii corresponding to each rare gas's van der Waals radius: 88.1% (argon), 79.1% (krypton) and 67.8% (xenon). The trend in this quantity goes in the same direction as that seen for the monolayer enhancement of electron emission shown in Table 2 suggesting that altered surface electron reflection probability is the dominant factor influencing the measured electron emission enhancement. This hypothesis is furthermore consistent with the observation that the maximum electron emission yield is seen for rare gas coverages substantially above a single monolayer. See Fig. 4.

Although a subtle feature of the data, it is interesting to note that Xe adlayers produce only about half the maximum electron emission efficiency compared to Ar or Kr. Whereas below 1 ML coverage the three rare gases adsorbate layers yield similar results, above one ML coverage, xenon exhibits no further enhancement – see Fig. 4. It is known from gas phase studies that small clusters of xenon atoms can form stable anions when the excess electron polarizes the cluster's closed electronic shell.[16] Accordingly, the electron affinity of equally sized clusters is significantly larger for xenon than for krypton or argon.[17] We explain the different behavior of xenon covered Au(111) by the electron affinity of the rare gas spacer: the xenon bilayer may be able to trap electrons (at least transiently) so that both ET to the CO* and reflection are reduced compared to Ar or Kr. This simple explanation qualitatively describes the underlying mechanism in accordance with our experimental observations. Studies using adsorbates with high electron affinity – like SF_6 – could help shed light on this hypothesis and are planned for the future.

It is also interesting to note the similarities of what is seen in this work with the elementary photo-physics of surface photo-chemistry. In this work, ET followed by electron emission quenches an excited molecule and leads to charge separation, leaving behind an electron hole at the surface. After photo-excitation, ET followed by charge separation is also believed to be a key step in surface photochemistry such as the photocatalytic splitting of water and methanol on TiO_2.[18–20] Here, photoexcitation of electrons from the valence band to the conduction band of TiO_2 creates electron hole-pairs, initiating the dissociation of surface adsorbates. It is widely accepted that fast thermalization of excited electrons to the conduction band edge and subsequent electron transfer to the adsorbates leads to the dissociation of water and methanol. However, recently Yu and coworkers found evidence that the dissociation does not occur on an electronically excited potential energy surface (PES) but on the ground state PES.[18] Clearly more work is needed to elucidate the underlying mechanism and to increase our knowledge about fundamental processes in photocatalysis. For this purpose, experiments on simple model systems can help to elucidate certain steps relevant for photocatalysis – such as charge separation and ET.

Molecular beam surface scattering experiments using diatomic molecules with well-defined surfaces allow studies of surface dynamics on the atomic scale. Simple model systems are chosen and compared with *ab initio* theory to understand general trends on a fundamental level.[21–24] Thus, the physical process of interest – in this case ET and charge separation – can be studied without

the influence of other degrees of freedom. Two experimental strengths should be noted when considering molecular beam surface scattering experiments. First, well-defined experimental conditions with complete control over the surface can be established by employing ultra-high vacuum (UHV) techniques. Second, the interaction of molecules with the surface can be studied with gas phase molecules. Hence, the impinging molecule can be prepared using optical methods in a well-defined quantum state allowing state-resolved experiments. It is our hope that these studies will help to further deepen our fundamental understanding of interfacial electron transfer and charge separation.

Conclusions

We investigated interfacial electron transfer and charge separation by scattering CO molecules in their $a^3\Pi$ state from rare gas covered Au(111). The rare gas adsorbates enhance electron ejection probability in comparison to clean Au(111). Maximum electron emission efficiencies close to unity are seen for Ar and Kr over-layers. These observations can be understood on the basis of an ET mediated auto-detachment mechanism. While the formation of the short-lived CO^- by electron transfer from the metal appears to be unaffected by 1–2 ML of rare gas adsorbate, the ejection of the electron into vacuum by auto-detachment from CO^- is dramatically influenced by surface coverage. An enhanced electron reflection probability of adsorbate covered surfaces helps explain the surprising observations of this work. We hope that these experimental studies will stimulate theoreticians to develop more sophisticated models for our observations.

Acknowledgements

Notes and references

1 N. Lorente, D. Teillet-Billy and J. P. Gauyacq, *Surf. Sci.*, 1999, **432**, 155–169.

2 P. Stracke, F. Wiegershaus, S. Krischok and V. Kempter, *Surf. Sci.*, 1998, **396**, 212–220.

3 F. Grätz, D. P. Engelhart, R. J. V. Wagner, H. Haak, G. Meijer, A. M. Wodtke and T. Schäfer, *Phys. Chem. Chem. Phys.*, 2013, **15**, 14951–14955.

4 F. Grätz, D. P. Engelhart, R. J. V. Wagner, G. Meijer, A. M. Wodtke and T. Schäfer, *J. Chem. Phys.*, 2014, **141**, 044712.

5 J. Marbach, F. X. Bronold and H. Fehske, *Phys. Rev. B: Condens. Matter Mater. Phys.*, 2011, **84**, 085443.

6 A. Hotzel, K. Ishioka, E. Knoesel, M. Wolf and G. Ertl, *Chem. Phys. Lett.*, 1998, **285**, 271–277.

7 C. Hückstädt, S. Schmidt, S. Hüfner, F. Forster, F. Reinert and M. Springborg, *Phys. Rev. B: Condens. Matter Mater. Phys.*, 2006, **73**, 075409.

8 L. Velarde, D. P. Engelhart, D. Matsiev, J. LaRue, D. J. Auerbach and A. M. Wodtke, *Rev. Sci. Instrum.*, 2010, **81**, 063106.

9 J. J. Gilijamse, S. Hoekstra, S. A. Meek, M. Metsälä, S. Y. T. van de Meerakker, G. Meijer and G. C. Groenenboom, *J. Chem. Phys.*, 2007, **127**, 221102.

10 D. P. Engelhart, F. Grätz, R. J. V. Wagner, H. Haak, G. Meijer, A. M. Wodtke and T. Schäfer, *Rev. Sci. Instrum.*, 2015, accepted.

11 R. D. Diehl, T. Seyller, M. Caragiu, G. S. Leatherman, N. Ferralis, K. Pussi, P. Kaukasoina and M. Lindroos, *J. Phys.: Condens. Matter*, 2004, **16**, S2839–S2862.

12 Y. Sonnenblick, E. Alexander, Z. H. Kalman and I. T. Steinberger, *Chem. Phys. Lett.*, 1977, **52**, 276–278.

13 L. Meyer, C. S. Barrett and P. Haasen, *J. Chem. Phys.*, 1964, **40**, 2744–2745.

14 J. Marbach, F. X. Bronold and H. Fehske, *Phys. Rev. B: Condens. Matter Mater. Phys.*, 2012, **86**, 115417.

15 H. J. Herlt and E. Bauer, *Surf. Sci.*, 1986, **175**, 336–368.

16 H. Haberland, T. Kolar and T. Reiners, *Phys. Rev. Lett.*, 1989, **63**, 1219–1222.

17 P. Stampfli, *Phys. Rep.*, 1995, **255**, 1–77.

18 C. Xu, W. Yang, Z. Ren, D. Dai, Q. Guo, T. K. Minton and X. Yang, *J. Am. Chem. Soc.*, 2013, **135**, 19039–19045.

19 A. Fujishima and K. Honda, *Nature*, 1972, **238**, 37–38.

20 A. L. Linsebigler, G. Lu and J. T. Yates, *Chem. Rev.*, 1995, **95**, 735–758.

21 I. Rahinov, R. Cooper, D. Matsiev, C. Bartels, D. J. Auerbach and A. M. Wodtke, *Phys. Chem. Chem. Phys.*, 2011, **13**, 12680–12692.

22 Y. Huang, C. T. Rettner, D. J. Auerbach and A. M. Wodtke, *Science*, 2000, **290**, 111–114.

23 N. H. Nahler, J. D. White, J. Larue, D. J. Auerbach and A. M. Wodtke, *Science*, 2008, **321**, 1191–1194.

24 J. D. White, J. Chen, D. Matsiev, D. J. Auerbach and A. M. Wodtke, *Nature*, 2005, **433**, 503–505.